HHS Public Access

Author manuscript

Structure. Author manuscript; available in PMC 2022 December 02.

The molecular basis of allostery in a facilitated dissociation process

Francis D. Appling, **Rebecca B. Berlow**, **Robyn L. Stanfield**, **H. Jane Dyson**, **Peter E. Wright**[*]
Department of Integrative Structural and Computational Biology and Skaggs Institute of Chemical Biology, Scripps Research, 10550 North Torrey Pines Road, La Jolla, CA, 92037.

Summary

Facilitated dissociation provides a mechanism by which high-affinity complexes can be rapidly disassembled. The negative feedback regulator CITED2 efficiently downregulates the hypoxic response by displacing the hypoxia inducible transcription factor HIF-1α from the TAZ1 domain of the transcriptional coactivators CBP and p300. Displacement occurs by a facilitated dissociation mechanism involving a transient ternary intermediate formed by binding of the intrinsically disordered CITED2 activation domain to the TAZ1:HIF-1α complex. The short lifetime of the intermediate precludes straightforward structural investigations. To obtain insights into the molecular determinants of facilitated dissociation, we model the ternary intermediate by generating a fusion peptide composed of the primary CITED2 and HIF-1α binding motifs. X-ray crystallographic and NMR studies of the fusion peptide complex reveal TAZ1-mediated negative cooperativity that results in nearly mutually exclusive binding of specific CITED2 and HIF-1α interaction motifs, providing molecular level insights into the allosteric switch that terminates the hypoxic response.

eTOC Blurb

The transcriptional response to hypoxia is regulated by a pair of disordered proteins, HIF-1α and CITED2. CITED2 downregulates HIF-1α-mediated transcription by competing for a shared molecular target by facilitated dissociation. Appling et al. model the intermediate of this process using a fusion peptide comprised of HIF-1α and CITED2 binding motifs.

Graphical Abstract

[*]**Lead Contact:** Further information and requests for resources and reagents should be directed to and will be fulfilled by the Lead Contact, Peter E. Wright (wright@scripps.edu).

Author Contributions

R.B.B., H.J.D., and P.E.W. conceived of the project. F.D.A., R.B.B., H.J.D., R.L.S., and P.E.W designed experiments. F.D.A., R.L.S., and R.B.B. performed experiments. F.D.A., R.L.S., R.B.B., H.J.D., and PEW analyzed data. F.D.A., R.B.B., H.J.D., and P.E.W. wrote the manuscript. All authors edited the manuscript and approved of the final version.

Declaration of Interests

The authors declare no competing interests.

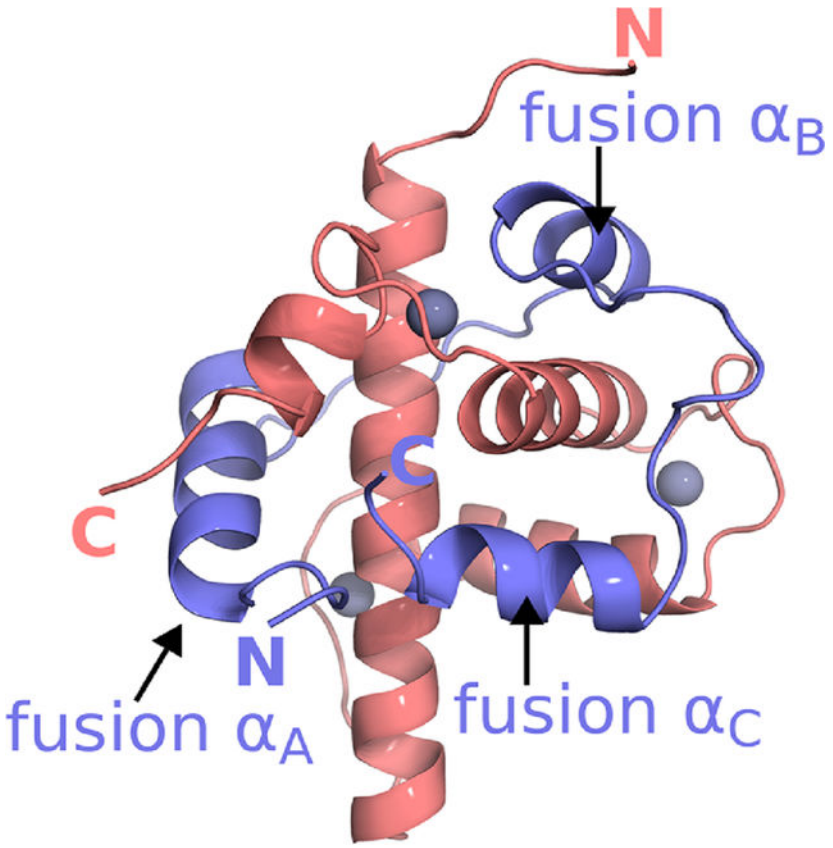

Keywords

hypoxic response; intrinsically disordered protein; transcriptional coactivator; competitive binding; allosteric switch; protein-protein interaction

Introduction

Dynamic protein-protein and protein-DNA interactions are central to the regulatory pathways of the cell. Activation and termination of cellular signaling processes is largely governed by the assembly and disassembly of regulatory complexes. Spontaneous, unimolecular dissociation of long-lifetime, high affinity regulatory complexes may be too slow to allow the cell to respond rapidly to changing conditions, and mechanisms have evolved to accelerate the process. Thus, many transcription factors can be actively removed from their DNA target sites by a “facilitated dissociation” or “molecular stripping” mechanism that decreases the lifetime of the DNA complex by enhancing the dissociation rate (Chen et al., 2018; Chen et al., 2015; Graham et al., 2010; Joshi et al., 2012; Kamar et al., 2017; Potoyan et al., 2017). Mechanistically, facilitated dissociation from DNA is aided by multivalent protein-DNA interactions that favor formation of transient ternary intermediates (Chen et al., 2018; Tsai et al., 2016). Facilitated dissociation of protein-protein complexes has also been reported, including accelerated displacement of an antigenic peptide from a Class II MHC complex and stimulated release of an IgE antibody from

the high affinity IgE Fc receptor in the presence of an engineered inhibitor (Kim et al., 2012; Schmitt et al., 1999). More recently, facilitated dissociation has been found to play a central role in termination of the cellular response to hypoxia (Berlow et al., 2017). In the present work we apply X-ray crystallography and NMR to elucidate the molecular mechanism of the allosteric switch that terminates the hypoxic response.

Evolution in an oxidizing environment has resulted in the development of regulatory networks that respond to O_2 levels and tune cellular metabolism to maintain homeostasis. At the center of the eukaryotic regulatory network is the heterodimeric transcription factor, hypoxia-inducible factor 1 (HIF-1) (Semenza, 2014). Under normoxic conditions, the α-subunit of HIF-1 (HIF-1α) is targeted for proteasomal degradation. In response to hypoxia, HIF-1α is stabilized and cellular HIF-1 levels rise rapidly to activate transcription of stress response genes (Huang et al., 1998; Ivan et al., 2001; Jaakkola et al., 2001; Semenza, 2014; Wang et al., 1995). Interactions between the intrinsically disordered C-terminal transactivation domain of HIF-1α and the TAZ1 domain of the general transcriptional coactivators CREB-binding protein (CBP) or its paralog p300 are essential for activation of HIF-1-mediated transcription (Arany et al., 1996; Ebert and Bunn, 1998). HIF-1 transcriptional activity is regulated through a negative feedback loop driven by the protein CITED2 (Bhattacharya et al., 1999; Henze and Acker, 2010). The gene encoding CITED2 is under the direct transcriptional control of HIF-1 and is strongly induced in response to hypoxia (Bhattacharya et al., 1999). The intrinsically disordered C-terminal activation domain of CITED2 competes with the C-terminal activation domain of HIF-1α for binding to TAZ1 to down-regulate HIF-1-mediated transcription.

The activation domain of HIF-1α folds upon binding to form three α-helices (HIF-1α-α_A, α_B, α_C) that partially encircle TAZ1 (Figure 1B) (Dames et al., 2002; Freedman et al., 2002). In contrast, CITED2 interacts with TAZ1 through a single N-terminal α-helix (CITED2-α_A) and an extended region that makes hydrophobic contacts with the TAZ1 α_1 and α_3 helices (Figure 1A) (De Guzman et al., 2004; Freedman et al., 2003). The HIF-1α and CITED2 activation domains occupy partially overlapping sites on TAZ1 and elicit TAZ1 conformations that differ in the C-terminal region of helix α_1 and in the length and orientation of helix α_4 (Figure 1). Although the HIF-1α and CITED2 activation domains exhibit little sequence homology, each possesses a 4-amino acid sequence, LP(Q/E)L, that makes similar interactions with TAZ1 in both complexes (Figures 1A, B). We have recently shown that HIF-1α and CITED2, through their competing interactions with TAZ1, function synergistically to form a hypersensitive, unidirectional regulatory switch that efficiently shuts off the hypoxic response (Berlow et al., 2017). The activation domain of CITED2 efficiently displaces the HIF-1α activation domain from the TAZ1:HIF-1α complex by an allosteric mechanism that greatly enhances the rate of HIF-1α dissociation. Remarkably, HIF-1α is ineffective at displacing CITED2 from its complex with TAZ1, even though the binary HIF-1α and CITED2 complexes with TAZ1 have identical affinities (K_d = 10 nM). Kinetic and NMR measurements showed that CITED2 facilitates dissociation of HIF-1α by formation of a transient ternary complex, in which HIF-1α and CITED2 bind simultaneously to TAZ1 and compete for binding of the conserved LP(Q/E)L motif (Berlow et al., 2017). The data suggested a model for the ternary complex in which CITED2 binds to TAZ1 through its α_A helix, displacing the weakly bound α_A region of HIF-1α, while

HIF-1α remains bound to TAZ1 through its α_B and α_C helices (Berlow et al., 2017; Berlow et al., 2019). However, since the CITED2 α_A and the HIF-1α α_B and α_C helices occupy non-overlapping surfaces of TAZ1, it is not readily apparent why the ternary complex is unstable and is formed only transiently. To reconcile these observations, a mechanism was proposed in which TAZ1-mediated allosteric interactions destabilize the ternary complex and facilitate dissociation of HIF-1α (Berlow et al., 2017).

Formation of the ternary complex is central to the displacement mechanism, but its transient nature has thus far precluded direct characterization of this intermediate in solution and has limited our ability to investigate the structural and dynamic properties that lead to the observed negative cooperativity of CITED2 and HIF-1α binding to TAZ1. To circumvent this problem, we generated a fusion peptide composed of the primary binding motifs of CITED2 and HIF-1α. In the complex between TAZ1 and the fusion peptide, the high local concentration of the CITED2 and HIF-1α binding motifs drives their association with TAZ1, enabling determination of the molecular basis of their competition. Using X-ray crystallography and solution NMR spectroscopy, we have characterized this model of the ternary intermediate to identify a critical component of the negative binding cooperativity between CITED2 and HIF-1α and to determine regions of TAZ1 that mediate the allosteric interaction. Our results provide detailed molecular insights into the mechanism of facilitated dissociation and further contribute to our understanding of how intrinsically disordered proteins compete for shared binding partners.

Results

Designing a CITED2-HIF-1α Fusion Peptide

To gain insights into the molecular mechanism by which CITED2 facilitates dissociation of HIF-1α from its complex with TAZ1, we generated a fusion peptide (Figure 1C) consisting of CITED2 α_A and LPEL (CITED2 residues 216–246; residues 6–36 in the fusion peptide) followed immediately by HIF-1α α_B and α_C (HIF-1α residues 796–826; residues 37–67 in the fusion peptide). We hypothesized that the fusion peptide would bind TAZ1 in a manner representative of the ternary complex, enabling us to define the structure and dynamics of the transient intermediate that govern the displacement process.

Crystal Structure of the TAZ1:fusion Peptide Complex

A crystal structure of the TAZ1:fusion peptide complex was determined to 2 Å resolution (Figure 2A). Data collection and refinement statistics are presented in Table 1. The fusion peptide wraps around TAZ1, with the CITED2 and HIF-1α motifs occupying the same binding sites on TAZ1 as in the parent binary complexes (Dames et al., 2002; De Guzman et al., 2004). A detailed comparison of the TAZ1:fusion peptide crystal structure with the NMR ensembles of the TAZ1:CITED2 and TAZ1:HIF-1α complexes (Dames et al., 2002; De Guzman et al., 2004) is shown in Figure S1. The structures of TAZ1 and the CITED2 and HIF-1α binding motifs are highly conserved in the fusion peptide complex. Although the overall structure of TAZ1 is very similar in all three complexes, local differences are observed at the C-terminal end of helix α_1, and in the length and orientation of the α_4 helix. The α_1 helix is slightly bent in the TAZ1:HIF-1α and TAZ1:CITED2 complexes, but is

visibly straightened in the TAZ1:fusion peptide complex. In the fusion peptide complex, the α_4 helix is of similar length to that in the TAZ1:HIF-1α complex but assumes the orientation observed in the TAZ1:CITED2 complex (Figure 2B). In addition, there are small shifts in the positions of the α_A and α_C helices of the fusion peptide relative to the binary CITED2 and HIF-1α complexes and pronounced structural differences in the C-terminal region of the α_C helix (Figure S1). In the binary TAZ1:HIF-1α complex, the HIF-1α C-terminal residues follow the trajectory of the α_C helix to place the free carboxyl terminus in an electropositive groove formed by the side chains of K365 and R368 on helix α_1. In contrast, residues F12 and I13 of the fusion peptide, N-terminal to the α_A helix, occlude this site in the crystal structure of the TAZ1:fusion peptide complex. The α_C helix of the fusion peptide is disrupted at D64 (equivalent to D823 in HIF-1α) and the last 3 residues project orthogonally towards the C-terminal end of the α_3 helix.

TAZ1 Conformational Exchange in the TAZ1:fusion Peptide Complex

High resolution NMR was used to probe the interactions between TAZ1 and the fusion peptide in solution. Two regions of the ^{1}H-^{15}N HSQC spectra of ^{15}N-labeled TAZ1 in complex with unlabeled CITED2, HIF-1α, or the fusion peptide are shown in Figure 3A and the full HSQC spectra are shown in Figure S2A. There are substantial differences between the spectra, reflecting differences both in the intermolecular interactions of the ligands and in the TAZ1 conformation in the various complexes. Approximately 80% of non-proline backbone amides of ^{13}C,^{15}N-labeled TAZ1 in complex with unlabeled fusion peptide were assigned from triple resonance spectra. In contrast, about 90% of TAZ1 backbone amides were assigned previously for the parent TAZ1:CITED2 and TAZ1:HIF-1α complexes (Dames et al., 2002; De Guzman et al., 2004).

Weighted average TAZ1 ^{1}H,^{15}N chemical shift differences between the TAZ1:fusion peptide complex and the TAZ1:CITED2 and TAZ1:HIF-1α complexes are plotted in Figure 3B. The chemical shift differences between the fusion and the CITED2 complexes are in general larger than those between the fusion peptide and HIF-1α complexes. Based on the structures in Figures 1A and 2, we would expect that regions of TAZ1 that contact α_A of CITED2 (TAZ1 helices α_1 and α_4) should show only small chemical shift differences between the CITED2 and fusion peptide complexes, whereas the regions that contact α_B and α_C of HIF-1α (N-terminus of α_1, C-terminus of α_2, and α_3 helix of TAZ1) should show only small chemical shift differences between the HIF-1α and fusion peptide complexes. Indeed, small chemical shift differences between the HIF-1α and fusion peptide complexes are observed for residues in the α_2 and α_3 helices (red bars in Figure 3B), confirming that these regions of TAZ1 have similar structure and similar intermolecular contacts in the HIF-1α and fusion peptide complexes, while larger differences are observed for residues in TAZ1 α_1 and α_4, as expected. The chemical shift differences between the CITED2 and fusion complexes (green bars in Figure 3B) differ greatly for residues in the α_2 and α_3 regions of TAZ1, also as expected from the structural data. However, the chemical shift differences of residues in α_1 are much larger than would be expected on the basis of the crystal structure, suggesting that in solution the interactions between TAZ1 and the fusion peptide α_A region differ from those in the TAZ1:CITED2 complex. In addition, there is a greater than 60% reduction in the heights of the Q355, V358, H362, H364, E370, and A372 amide cross

peaks in the HSQC spectrum of the fusion complex compared to that of the TAZ1:CITED2 complex (Figure S2B). These residues lie on the face of the TAZ1 α_1 helix that contacts the α_A region of the fusion peptide (Figure 3C), suggesting the possibility of exchange broadening due to conformational fluctuations in the molecular interface (see following section).

In the crystal structure of the fusion peptide complex, the TAZ1 α_4 helix assumes the length observed in the HIF-1α complex and the orientation observed in the CITED2 complex (Figure 2B). Consistent with this observation, chemical shift differences are observed between the fusion peptide complex and both parent complexes for residues in the TAZ1 α_4 helix (Figure 3B). The relative magnitudes of the α_4 chemical shift differences indicate that the conformation of the TAZ1 α_4 helix in the fusion peptide complex differs from that in the HIF-1α complex but does not fully achieve the length and/or conformation observed in the CITED2 complex. These observations are directly reflected in the HSQC spectra (Figure 3A), where cross peaks corresponding to TAZ1 α_4 helix residues A435 (left panel) and S436 (right panel) are shown. In the spectrum of the TAZ1:fusion peptide complex (blue), these cross peaks are shifted away from their positions in the TAZ1:HIF-1α spectrum (red) towards their positions in the TAZ1:CITED2 spectrum (green). The A435 and S436 cross peaks in the three spectra (TAZ1:CITED2, TAZ1:HIF-1α, and TAZ1:fusion peptide) fall roughly on a line, suggesting that TAZ1 in the fusion peptide complex likely undergoes a fast exchange process in which the α_4 helix interconverts between its conformation in the HIF-1α complex and its conformation in the CITED2 complex.

Fusion Peptide Conformational Exchange in the TAZ1 Complex

The exchange process in the TAZ1:fusion peptide complex was further probed by solution NMR investigation of the isotopically-labeled fusion peptide in complex with unlabeled TAZ1. An overlay of the amide region of ^{1}H-^{15}N HSQC spectra of free and TAZ1-bound ^{15}N-labeled fusion peptide is shown in Figure 4A. The limited ^{1}H chemical shift dispersion of the free fusion peptide spectrum shows that it, like the parent CITED2 and HIF-1α activation domains, is intrinsically disordered. The chemical shift dispersion is increased upon binding to TAZ1, indicating folding of the fusion peptide. However, the amide cross peaks of the bound fusion peptide exhibit heterogenous intensities (Figure 4B) and only 49 of the expected 64 backbone amide cross peaks are observed in spectra of ^{15}N-labeled fusion peptide in complex with unlabeled TAZ1.

The heterogeneity of the cross-peak intensities suggests that exchange broadening is non-uniform across the fusion peptide and is particularly severe for residues in the α_A region, where cross peaks are broadened beyond detection. The amide cross peaks of residues 13–18, 20 and 21 in the α_A region of TAZ1-bound CITED2 (using the numbering of the fusion peptide from Figure 1) are intense and well-resolved (Figure S3). However, the corresponding cross peaks are entirely missing from spectra of the fusion peptide complex (Figures 5A and S3A), consistent with exchange broadening due to conformational fluctuations in the N-terminal region of α_A, where it contacts the TAZ1 α_1 helix (Figure 3C). The amide cross peaks associated with residues 22–31 of the bound fusion peptide are generally weak but are observed at chemical shifts that are similar to those of the

corresponding residues of the CITED2 binary complex (Figure S3A). Residues L21 – M25 adopt helical structure in both the fusion peptide and CITED2 complexes, based on their similar $^{13}C\alpha$ chemical shifts. The chemical shifts of residues 38–49, 52–59, 61, 64, and 67 of the bound fusion peptide are very close to those of HIF resonances in the binary TAZ1:HIF complex (Figure S3A). However, the resonances of several α_C residues (60, 63, 65, 66) also exhibit exchange broadening, resulting in low signal intensity (Figure 4B). The differential broadening observed for both fusion peptide and TAZ1 resonances (Figure 3C) provides strong evidence for enhanced conformational exchange relative to the binary complexes in the α_A and α_C regions of the TAZ1-bound fusion peptide and in the regions of TAZ1 (α_1 and α_4 helices) that they contact, suggesting that co-occupation of TAZ1 by the α_A helix of CITED2 and the α_C helix of HIF-1α is unfavorable, i.e. that binding is mutually antagonistic.

Negative Allosteric Modulation of α_A and α_C Binding

To test the hypothesized antagonistic binding of the α_A and α_C regions of the fusion peptide, we performed site-directed mutagenesis to introduce Leu to Ala substitutions designed to impair binding of the α_A (L21A) or α_C (L63A) helices by disrupting hydrophobic interactions with TAZ1. L21 packs into a hydrophobic pocket formed by V358 in the TAZ1 α_1 helix and L432 and A435 in the TAZ1 α_4 helix, while L63 makes hydrophobic contacts with L360 and L361 in the TAZ1 α_1 helix and I415 in the TAZ1 α_3 helix (Figure S4A). ^1H-^{15}N HSQC spectra of ^{15}N labeled L21A and L63A fusion peptides free in solution and bound to unlabeled TAZ1 are shown in Figure S4B,C. Overlays of the ^1H-^{15}N HSQC spectra of the TAZ1 complexes of HIF-1α, CITED2 and the mutant peptides are shown in Figures 5B, S3B,C. Weighted average backbone ^1H,^{15}N chemical shift differences between the original and the mutant fusion peptides in complex with TAZ1 are plotted in Figure 6A. The differences between the two sets of chemical shift differences are striking. The L21A substitution results in only very small chemical shift changes relative to the original fusion peptide complex, whereas dramatic chemical shift changes are observed for residues in the N- and C-terminal regions of the fusion peptide in response to the L63A substitution (Figure 6A). In addition, the L63A substitution results in a decrease in the exchange broadening observed in spectra of the original fusion peptide in complex with TAZ1, enabling observation of backbone amide resonances corresponding to the α_A region and assignment using standard triple resonance experiments.

Upon binding to TAZ1, residues in the α_A and α_B regions of the L63A peptide experience large changes in backbone amide chemical shifts (black bars in Figure 6B), indicating interactions with TAZ1 and folding of the peptide. In contrast, amide cross peaks of residues in the C-terminal region (G49 – N67) are largely unperturbed by binding, showing that this region does not interact with TAZ1 and that the α_C helix remains unfolded and disordered. Comparison of the ^1H-^{15}N HSQC spectrum of the L63A fusion peptide complex with the spectra of the TAZ1:CITED2 and TAZ1:HIF-1α complexes provides additional insights. The green bars in Figure 6B show that the chemical shifts of backbone amides of residues 9–35 of the L63A fusion peptide bound to TAZ1 are very similar to those of the corresponding residues of the CITED2-TAZ1 complex (residues 219–245, see Figures 5B and S3C), confirming that the α_A helix of the L63A peptide folds and makes intimate

contacts with TAZ1 in a similar manner to the α_A helix of CITED2. Additionally, the chemical shifts of backbone amides of residues 40–45 of the TAZ1-bound L63A fusion peptide are very similar to those of the corresponding residues (HIF-1α 795–804, Figure S3C) in the HIF-1α complex (red bars in Figure 6B), showing that the α_B region adopts the same structure and makes similar TAZ1 contacts in both the L63A fusion peptide and HIF-1α complexes. However, residues 50–67 of the TAZ1-bound L63A fusion peptide show large backbone amide chemical shift differences from the corresponding residues (HIF-1α 809–826) of the HIF-1α complex. The backbone amide cross peaks of residues 50–67 have nearly identical ^{1}H and ^{15}N chemical shifts to those of the free L63A peptide ($\Delta\delta_{ave} < 0.07$ ppm), indicating dissociation of α_C and the α_B–α_C loop from the surface of TAZ1. From these observations we conclude that the L63A substitution largely abrogates the folding of α_C and its interaction with TAZ1, while simultaneously enhancing binding of α_A to stabilize the helical structure observed in the TAZ1:CITED2 complex in solution and in the TAZ1:fusion peptide complex in the crystal (Figures 1A, 2A).

In contrast to the large differences observed between the L63A fusion complex and the TAZ1:HIF-1α complex, comparison of the backbone amide chemical shifts for the L21A fusion complex with those of the TAZ1:HIF-1α complex (Figure S5) shows that the α_B and α_C regions of the L21A peptide are stably bound and adopt similar conformations in the two complexes. In common with the unmodified fusion peptide, backbone amide cross peaks of α_A residues are exchange-broadened in the spectrum of the L21A peptide complex. Thus, the mutagenesis experiments clearly show that, in solution, binding of the α_A and α_C helices is mutually exclusive; the two helices in the fusion peptide cannot bind simultaneously while making optimal contacts with TAZ1. When the α_C helix is bound, interactions with the α_A region are weak and transient and lead to exchange broadening in the spectrum of the fusion peptide complex. Conversely, impairment of the capacity for α_C helix binding, as observed in the L63A fusion peptide complex, allows folding and binding of the α_A helix.

The α_A helix is stabilized by lattice contacts in the crystal

Given the antagonism observed in binding of the α_A and α_C helices to TAZ1 in solution, it is at first surprising that both helices are fully folded and docked to TAZ1 in the crystal structure of the fusion peptide complex (Figure 2A). However, examination of the packing in the crystal lattice reveals that the α_A helix is sandwiched between its binding site on TAZ1 and the α_2 helix of a neighboring TAZ1 molecule (Figure S6). This configuration in the crystal promotes docking of the α_A helix to its binding site and enables observation of a complex in which both the α_A and α_C helices are docked.

Mechanism of TAZ1-Mediated Allostery

To identify the regions of TAZ1 that mediate the negative allostery observed in binding of the α_A and α_C helices of the fusion peptide, we used NMR to characterize the complexes of ^{15}N-labeled TAZ1 with the L21A and L63A fusion peptides. Comparison of the ^{1}H-^{15}N HSQC spectra of the original and L63A fusion peptide complexes (shown in Figure S7) reveals larger than average chemical shift differences for residues located in the TAZ1 α_4 helix and in the α_C binding site, at the interface of the α_1, α_2, and α_3 helices of TAZ1 (Figure 7A). The observed chemical shift changes provide further evidence that loss of

hydrophobic contacts due to the L63A substitution weakens the interactions between TAZ1 and α_C and promotes dissociation of the α_C helix. In contrast, the L21A mutation causes little change in the TAZ1 backbone amide chemical shifts except at the C-terminal end of the α_4 helix (Figure 7A).

The cross peaks of A435 and S436 in the spectrum of the fusion peptide complex report on the state of TAZ1 α_4. In the fusion peptide complex, these cross peaks are located at chemical shifts intermediate between their positions in the spectra of the TAZ1:HIF-1α and TAZ1:CITED2 complexes (Figure 3A). The L21A and L63A substitutions have opposite effects on these cross peaks: the L21A substitution shifts both cross peaks towards their positions in the TAZ1:HIF-1α spectrum whereas the L63A substitution shifts them to positions that are nearly coincident with the corresponding cross peaks in the TAZ1:CITED2 spectrum (Figure 7B).

The orientation and length of the TAZ1 α_4 helix is sensitive to the identity of the bound ligand and is shorter in the TAZ1:HIF-1α and TAZ1:fusion peptide complexes than in the TAZ1:CITED2 complex (Figure 2B). To determine whether the L21A and L63A mutations affect the hydrogen-bonded helical structure of α_4, we measured backbone amide proton chemical shift temperature coefficients to probe the propensity for formation of intramolecular hydrogen bonds (Baxter and Williamson, 1997). The temperature coefficients of the amide proton chemical shifts of A378 and S411, representing solvent exposed and hydrogen bonded controls, respectively, and two residues in α_4, A435 and S436, are shown in Figure 6C and the fitted data are shown in Figure S8. The temperature coefficient of the A378 amide proton resonance (≈ −7 ppb K^{-1}) is consistent with its solvent-exposed position while that of the S411 amide (≈ 0 ppb K^{-1}) is characteristic of an amide proton involved in an intramolecular hydrogen bond. The temperature coefficients of A378 and S411 in the fusion peptide complex are unaffected by the L21A and L63A mutations. In contrast, the temperature coefficients of A435 and S436 are more negative than −5 ppb K^{-1} in both the fusion peptide and L21A peptide complexes but become more positive (≈ −3.5 and ≈ −1.5 ppb K^{-1} for A435 and S436, respectively) in the L63A peptide complex. These data are consistent with A435 and S436 being largely solvent exposed (ie, α_4 unfolded) in the original and L21A fusion peptide complexes but engaged in intramolecular hydrogen bonds when TAZ1 is bound to the L63A fusion peptide. Figures 7B and C provide strong evidence that binding and folding of the fusion peptide α_A and α_C helices are both linked to the TAZ1 α_4 helix folding equilibrium. Binding of the CITED2 α_A helix extends and stabilizes the TAZ1 α_4 helix whereas binding of the HIF-1α α_C helix destabilizes α_4, suggesting that the α_4 region plays a central role in mediating the negative allostery observed in binding of the α_A and α_C helices of the fusion peptide.

Discussion

Previous studies have shown that the negative feedback regulator CITED2 efficiently displaces HIF-1α from its complex with the TAZ1 domain of CBP/p300 by an associative mechanism involving formation of a transient ternary complex (Berlow et al., 2017). The present work provides insights into the nature of the ternary complex and reveals the

structural basis for the negative allosteric coupling between the CITED2 α_A and HIF-1α α_C binding sites that promotes HIF-1α dissociation.

The ternary complex was modeled using an engineered fusion peptide consisting of the CITED2 α_A-LPEL and HIF-1α α_B and α_C motifs. In contrast to the crystal structure of the TAZ1:fusion peptide complex, where crystal packing stabilizes the interactions between TAZ1 and the CITED2 α_A helix, NMR measurements show that contacts between the α_A region and TAZ1 are weak and highly dynamic in solution. The C-terminal end of α_C also shows exchange broadening in the fusion complex (Figures 4B, 5A, S3A), even though the HIF-1α α_B and α_C helices dominate the interaction between the fusion peptide and TAZ1. This observation suggests that the α_C interactions are weakened compared to those in the parent TAZ1:HIF-1α complex (Berlow et al., 2017; Berlow et al., 2019; Dames et al., 2002). The NMR data for the complexes formed by the original fusion peptide and the L21A and L63A mutants show that binding of the HIF-1α α_C helix antagonizes interactions with the CITED2 α_A helix and *vice versa*. This negative allostery appears to be mediated by the α_4 helix of TAZ1, which differs in length and orientation depending upon whether CITED2 or HIF-1α is bound. The α_4 folding equilibrium is driven in opposite directions: binding of CITED2 α_A to TAZ1 stabilizes an extended α_4 helix, whereas binding of HIF-1α α_C to TAZ1 promotes unfolding of α_4. The opposing effects of CITED2 α_A and HIF-1α α_C binding on the TAZ1 α_4 folding equilibrium are a likely source of the observed negative allostery between CITED2 and HIF-1α binding.

The conformational plasticity of TAZ1 plays a central role in the competition between the CITED2 α_A and HIF-1α α_C helices for binding to TAZ1 (Berlow et al., 2017; Berlow et al., 2019; Ruiz-Ortiz and De Sancho, 2020). NMR relaxation measurements and molecular dynamics simulations reveal fast timescale dynamics in the α_4 region of free TAZ1 and the TAZ1:HIF-1α complex that are damped in the binary CITED2 complex (Berlow et al., 2019; Ruiz-Ortiz and De Sancho, 2020), where interactions with the α_A helix stabilize extension of helical structure in α_4. We propose that allostery arises through thermodynamic coupling that modulates the population of binding-competent states. CITED2 α_A binding to TAZ1 increases the population of fully extended α_4 helix, which decreases the affinity of the TAZ1–HIF-1α α_C interaction. On the other hand, HIF1α α_C binding to TAZ1 decreases the population of the extended TAZ1 α_4 helix, thereby impairing the TAZ1-CITED2 α_A interaction. Therefore, the equilibria of CITED2 α_A-TAZ1 and HIF-1α α_c-TAZ1 binding interactions are coupled to one another through their individual linkages to the TAZ1 α_4 folding equilibrium. Importantly, while the discussion here has focused on the linkage between α_A/α_C binding and TAZ1 α_4 extension, it is important to remember that CITED2 α_A and HIF-1α α_C are both disordered in solution and must fold upon binding to TAZ1. The CITED2 α_A and HIF-1α α_C folding equilibria are thus integral components of the network of linked equilibria that determine the outcome of allosteric interactions between α_A and α_C on the surface of TAZ1.

A number of studies using coarse-grained molecular dynamics simulations to probe the mechanism by which CITED2 drives displacement of HIF-1α from TAZ1 have recently been published (Chu et al., 2020; Ruiz-Ortiz and De Sancho, 2020; Wang and Brooks, 2020). In each of these simulations, the displacement reaction was observed to proceed

through an intermediate in which CITED2 is essentially fully bound to TAZ1 while HIF-1α is bound only through α_C, with the α_A and α_B regions fully dissociated. Due to the design of the fusion peptide, the α_B and α_C helices of HIF-1α both remain bound to TAZ1 in our current model of the ternary complex, which thus represents an earlier step on the displacement pathway than the intermediate observed in the molecular dynamics simulations. It is probable that the hydrophobic residues immediately C-terminal to the LPEL motif of CITED2, which bind in the α_B site but are absent from the fusion peptide, play an important role in HIF-1α displacement by competing with the α_B helix for binding to TAZ1. These additional hydrophobic contacts would be expected to strengthen the TAZ1:CITED2 interactions, weaken HIF-1α binding by displacing α_B, and shift the TAZ1 α_4 folding equilibrium towards the CITED2-bound state. Given the negative allostery between the α_A and α_C binding sites revealed by our current experiments, the enhanced interactions with the CITED2 α_A helix would destabilize binding of the HIF-1α α_C helix and facilitate dissociation of HIF-1α.

Intrinsically disordered proteins and protein regions constitute a large fraction of the human proteome and are overrepresented in eukaryotic transcriptional regulation and cell signaling pathways (Iakoucheva et al., 2002; Liu et al., 2006; Wright and Dyson, 2015). Given the ubiquity of IDPs, it is unlikely that the facilitated dissociation mechanism regulating the interactions between TAZ1, CITED2, and HIF-1α is unique. Indeed, facilitated dissociation of the disordered histone H1 – prothymosin α complex involving transient ternary complex formation has recently been reported (Borgia et al., 2018; Sottini et al., 2020). Many IDPs contain multiple binding motifs that engage their targets with varying strengths of interaction, enabling the formation of multivalent complexes with non-uniformly distributed binding energy (Berlow et al., 2015; Wright and Dyson, 2015). It is clear that the machinery required for facilitated dissociation is a hallmark of IDPs and it therefore seems likely that many signaling hubs involving IDPs engage in facilitated dissociation. Facilitated dissociation provides a mechanism by which high affinity, long lifetime complexes can be rapidly disassembled. Importantly, this allows for stable “on” signals *and* fast “off” signals. This is precisely the type of switch-like behavior observed in the TAZ1 / CITED2 / HIF-1α system (Berlow et al., 2017). Both CITED2 and HIF-1α bind to TAZ1 with nanomolar affinity and display slow intrinsic dissociation kinetics (Berlow et al., 2017; Lindström et al., 2018). Without accelerated displacement of HIF-1α by CITED2, the rapid on/off switching characteristic of the hypoxic response would not be possible.

While the hypoxic response is an essential component of human physiology, it is often co-opted by cancer cells, which are generally hypoxic, to promote tumor growth and metastasis (Bertout et al., 2008; Nurwidya et al., 2012; Semenza, 2014). Knowledge of the molecular details of the hypoxic response could be fruitful for the design of therapeutics: the crystal structure of the model ternary intermediate in CITED2-driven displacement of HIF-1α presented in this work should prove useful to the design of small molecule modulators of the displacement reaction. Importantly, we have defined specific interactions within the complex that strengthen or weaken the interaction between TAZ1 and either of its binding partners, providing the opportunity to steer the reaction and the regulatory pathway. Therefore, our findings not only represent a detailed molecular-level dissection of an allosteric network involving IDPs but also provide an avenue for highly targeted therapeutic design.

STAR Methods Text

Resource Availability

Lead Contact—Further information and requests for resources and reagents should be directed to and will be fulfilled by the lead contact, Peter E. Wright wright@scripps.edu

Materials Availability—Plasmids generated in this study have been deposited to Addgene. Catalog numbers are given in the key resources table.

Data and Code Availability

- Chemical shift assignment data have been deposited at the BioMagResBank, and coordinates and structure factors have been deposited at the PDB, and are publicly available as of the date of publication. Accession numbers are listed in the key resources table.
- This paper does not report original code.
- Any additional information required to reanalyze the data reported in this paper is available from the lead contact upon request.

Experimental Model and Subject Details

Source Organism.—*Escherichia coli* BL21(DE3) (DNAY); *Escherichia coli* XL-1 Blue competent cells. Culture conditions include LB medium and minimal (M9) medium supplemented with stable isotope labeled precursors as described in detail below.

Method Details

Sample Preparation.—The CITED2-HIF-1α fusion peptide was generated by cloning the sequence coding for human CITED2 residues 216–246 followed immediately by the sequence coding for human HIF-1α residues 796–826 into a co-expression vector with TAZ1 (mouse CBP residues 340–439). The fusion peptide sequence was cloned into the vector immediately downstream of the sequence coding for N-terminally His_6-tagged GB1 (Sugase et al., 2008). Site-directed mutagenesis to generate the L21A and L63A fusion peptide constructs was accomplished using standard QuikChange PCR protocols.

The CITED2 C-terminal transactivation domain (residues 216–269 of human CITED2), the HIF-1α C-terminal transactivation domain (residues 776–826 of human HIF-1α), and the CITED2-HIF-1α fusion peptide constructs were expressed in *E. coli* BL21 (DE3) [DNAY] as His_6-tagged GB1 fusion proteins in a coexpression vector with TAZ1 (residues 340–439 of mouse CBP). Cells were grown in M9 minimal media. Cells were cultured at 37 °C to OD_{600} ~ 0.8 at which time protein expression was induced by the addition of ~ 1 mM IPTG and ~ 100 μM $ZnSO_4$ and growth was continued at 18 °C for an additional 18–21 hours. Cells were harvested by centrifugation at 4 °C and cell pellets were stored at −20 °C prior to protein purification. Cell pellets were resuspended in 40 mL of buffer containing 25 mM Tris pH 8.0, 200 mM NaCl, 8 M urea, and 20 mM imidazole per liter of culture and lysed by sonication at 4 °C. The soluble fraction was isolated by centrifugation at 4 °C. The supernatant was purified at room temperature by nickel affinity chromatography using

NiNTA resin and the HIF-1α and CITED2 peptides were separated from the His_6-GB1 tag by thrombin cleavage on the resin. The cleaved HIF-1α, CITED2 and fusion peptides were further purified by reversed phase HPLC, using a C4 cartridge (Waters) in acetonitrile/0.1% TFA mobile phase. Pure peptides were lyophilized and stored at −20 °C. Lyophilized peptides were dissolved in 50 – 100 mM Tris buffer pH 8 ~ 10 mM DTT and dialyzed overnight against buffer containing 20 mM Tris pH 6.8, 50 mM NaCl, and 2mM DTT prior to use (Berlow et al., 2017). . After removal of the the His_6-GB1 tag by thrombin cleavage, the sequence GSHMS remained at the N-terminus of the CITED2 and fusion peptides and the sequence GSHM at the N-terminus of HIF-1α. TAZ1 was expressed and purified under native conditions. *E. coli* BL21(DE3) [DNAY] were grown in M9 minimal medium at 37°C to OD_{600} ~ 0.8. Protein expression was induced by addition of 1 mM IPTG and ~ 100 μM $ZnSO_4$ and growth was continued at 18°C for an additional 18–21 hours. Cells were harvested by centrifugation at 4 °C and cell pellets were stored at −20 °C prior to protein purification. Cells were resuspended in ice-cold buffer (40 mL per liter of cell culture) containing 20 mM Tris pH 8, 40 mM NaCl, 10 μM $ZnSO_4$, 10 mM DTT, and Pierce EDTA-free protease inhibitor cocktail (1 tablet / 150 mL buffer) and lysed by sonication. The soluble lysate fraction was loaded onto HiTrapQ and HiTrapSP columns (GE Healthcare) connected in series that were pre-equilibrated in 20 mM Tris pH 8, 40 mM NaCl, 10 μM $ZnSO_4$, and 2mM DTT. The columns were washed until the UV absorbance at 280 nm returned to baseline. The HiTrapQ column was then removed and bound TAZ1 was subsequently eluted from the HiTrapSP column using a linear gradient to 600mM NaCl in 20 mM Tris pH 8. Fractions containing nearly pure TAZ1 were then further fractionated by size exclusion chromatography on a Superdex75 column (Amersham Biosciences) in 20 mM Tris pH 8, 200 mM NaCl, and 2 mM DTT. Aliquots of pure TAZ1 were made ~ 10 mM in DTT using 1 M DTT stocks, flash frozen with liquid nitrogen, and stored at −80 °C.

TAZ1 and fusion peptides were uniformly labeled with ^{15}N or ^{15}N,^{13}C by expression in M9 minimal media containing $^{15}NH_4Cl$ (1 g L^{-1}) or $^{15}NH_4Cl$ (0.5 g L^{-1}) /^{15}N H_4SO_4 (0.5 g L^{-1}) as the sole nitrogen sources and ^{13}C glucose (2.5 g L^{-1}) as the sole carbon source.

Protein concentrations were determined by measuring absorbance at 280 nm and using extinction coefficients of 1490 $M^{-1}cm^{-1}$ for HIF-1α and fusion peptide constructs and 5500 $M^{-1}cm^{-1}$ for TAZ1 and CITED2. Extinction coefficients were calculated using the ExPASy ProtParam web server.

Samples for NMR and crystallography were prepared by dialysis at 4 °C into NMR/crystallography buffer: 20 mM Tris-Cl pH 6.8, 50 mM NaCl, 2 mM DTT. D_2O was added to NMR samples to achieve 5%.

Crystallization and Structure Analysis.—The TAZ1:fusion peptide complex was prepared at a 1:1 TAZ1:peptide molar ratio at 1.2 mM in NMR/crystallography buffer and was crystallized by sitting drop vapor diffusion at 20 °C with a precipitant of 0.1 M HEPES pH 6.87, 28% (w/v) PEG 4000. Crystals were cryoprotected in 30% ethylene glycol / 70% well solution before flash-cooling in liquid nitrogen. Crystallographic data (2.0 Å resolution) were collected at 100 K at the Advanced Light Source at Lawrence Berkeley National Laboratory on Beamline 5.0.3. Data were processed and scaled with the HKL-2000 software

suite (Otwinowski and Minor, 1997) in space group $P2_1$ with unit cell dimensions 32.06, 50.11, 41.26 and β=99.19. An incomplete polyalanine model consisting of 79 residues (395 atoms) in 6 chains with a CC of 33.5% was generated using Arcimboldo Lite (Rodriguez et al., 2009). The lowest energy NMR structure of TAZ1 (1U2N (De Guzman et al., 2005)) was aligned to the polyalanine model and used as a starting model for refinement. The model was iteratively refined and re-built using Phenix (Liebschner et al., 2019) and Coot (Emsley et al., 2010). The final model contains 155 residues (1213 protein atoms) in 2 chains with 38 modeled waters and 3 Zn atoms. Validation was carried out with Molprobity (Williams et al., 2018) with 94.7%/0.66% of residues in favored/outlier regions of the Ramachandran plot. Structural statistics are listed in Table 1.

NMR Spectroscopy.—NMR spectra were acquired at 298 K, unless otherwise noted, on a Bruker Avance 900 MHz spectrometer with a room temperature triple resonance probe and Bruker Avance 500 and 700 MHz spectrometers equipped with triple resonance cryoprobes. Complexes were prepared by combining isotope labeled TAZ1 or peptide in NMR/crystallography buffer with a 1.2−1.9 fold excess of unlabeled peptide or TAZ1 in the same buffer. Spectra for determining resonance assignments for TAZ1:fusion peptide complexes were acquired at 300 μM – 400 μM concentration of isotope-labeled component. Spectra for determining resonance assignments for the free fusion peptide were obtained at 100 μM concentration. Resonance assignments for TAZ1:CITED2 and TAZ1:HIF-α complexes have been reported previously (Dames et al., 2002; De Guzman et al., 2004). All other NMR experiments utilized 100 μM labeled component.

Backbone resonance assignments for the free and bound fusion peptide, the bound L63A fusion peptide, and TAZ1 bound to the original and L63A fusion peptides were obtained from HNCA, HN(CO)CA, HNCO, HN(CA)CO, HNCACB, and HN(CO)CACB triple resonance spectra (Sattler et al., 1999) as implemented in the TopSpin 3.2 pulse program library. Assignments for the free L63A fusion peptide were made by comparing the ^{1}H-^{15}N HSQC spectra of the L63A and original fusion peptides. Based on the similarity of the spectra, assignments for resolved cross peaks of ^{15}N-labeled TAZ1 in complex with unlabeled L21A fusion peptide were transferred from the ^{1}H-^{15}N HSQC spectrum of the original fusion peptide complex. Similarly, assignments of the bound L21A peptide were transferred from those of the unmodified fusion peptide complex. Triple resonance spectra of free isotopically labeled original fusion peptide as well as isotopically labeled TAZ1 bound to unlabeled original fusion peptide were collected using band-selective amide proton pulses (Lescop et al., 2007; Schanda et al., 2006). The indirect dimensions were uniformly sampled and doubled in size by zero filling. All triple resonance spectra were reconstructed using iterative soft thresholding (Drori, 2007; Stern et al., 2007). NMR data were processed using NMRPipe (Delaglio et al., 1995) and spectra were visualized using SPARKY (Lee et al., 2015) on the NMRbox platform (Maciejewski et al., 2017).

Quantification and Statistical Analysis

Weighted average ^{1}H,^{15}N chemical shift differences were calculated as described in the Figure 3 legend. The 10 % trimmed means and standard deviations of chemical shift difference data sets were determined by calculating the 0.9 quantile of a given data set using

GNU Octave, generating a list of chemical shift differences less than the 0.9 quantile, and calculating the mean and standard deviation of this trimmed data set. Where indicated in the figure legends, broken lines inside graphs of chemical shift differences report the sum of the 10 % trimmed mean and standard deviation.

Intensities of cross peaks from ^{1}H-^{15}N-HSQC spectra were obtained using Sparky and were normalized as described in the Figure S2 legend.

^{1}H chemical shift temperature coefficients were calculated by determining the slopes of ^{1}H chemical shift Vs. temperature data using linear regression scripts written in GNU Octave ($\beta_0 = \overline{CS} - \beta_1\bar{T}$; $\beta_1 = \frac{\sum_i (T_i - \bar{T})(CS_i - \overline{CS})}{\sum_i (T_i - \bar{T})^2}$; $CI_{68} = t_{68}\sqrt{\frac{MSR}{\sum_i (T_i - \bar{T})^2}}$, where β_0 and β_1 denote the intercept and ^{1}H chemical shift temperature coefficient respectively, T_i and CS_i denote the i^{th} temperature and chemical shift respectively, CI_{68} denotes the 68 % confidence interval of the ^{1}H chemical shift temperature coefficient, t_{68} denotes the 68 % single-tailed critical value of the t-distribution, MSR denotes the sum of squared residuals divided by the degrees of freedom, and overbars denote averages).

Additional Resources

See Key Resources Table.

Supplementary Material

Refer to Web version on PubMed Central for supplementary material.

Acknowledgments

We thank Gerard Kroon for assistance with NMR experiments, Euvel Manlapaz for technical assistance, Mary Lonsdale for assistance in collecting preliminary data, Maria Martinez-Yamout for assistance with HPLC, Henry Tien for assistance with robotic crystallization, and Wright/Dyson lab members for insightful discussions. This work was supported by Grants CA096865 and CA229652 (PEW) and GM131693 (HJD) from the National Institutes of Health and the Skaggs Institute for Chemical Biology. The Berkeley Center for Structural Biology is supported in part by the Howard Hughes Medical Institute. The Advanced Light Source is a Department of Energy Office of Science User Facility under Contract No. DE-AC02-05CH11231.

References

Arany Z, Huang LE, Eckner R, Bhattacharya S, Jiang C, Goldberg MA, Bunn HF, and Livingston DM (1996). An essential role for p300/CBP in the cellular response to hypoxia. Proc. Natl. Acad. Sci. U.S.A 93, 12969–12973. [PubMed: 8917528]

Baxter NJ, and Williamson MP (1997). Temperature dependence of ^{1}H chemical shifts in proteins. J. Biomol. NMR 9, 359–369. [PubMed: 9255942]

Berlow RB, Dyson HJ, and Wright PE (2015). Functional advantages of dynamic protein disorder. FEBS Lett 589, 2433–2440. [PubMed: 26073260]

Berlow RB, Dyson HJ, and Wright PE (2017). Hypersensitive termination of the hypoxic response by a disordered protein switch. Nature 543, 447–451. [PubMed: 28273070]

Berlow RB, Martinez-Yamout MA, Dyson HJ, and Wright PE (2019). Role of backbone dynamics in modulating the interactions of disordered ligands with the TAZ1 domain of the CREB-binding protein. Biochemistry 58, 1354–1362. [PubMed: 30775911]

Bertout JA, Patel SA, and Simon MC (2008). The impact of O_2 availability on human cancer. Nat. Rev. Cancer 8, 967–975. [PubMed: 18987634]

Bhattacharya S, Michels CL, Leung MK, Arany ZP, Kung AL, and Livingston DM (1999). Functional role of p35srj, a novel p300/CBP binding protein, during transactivation by HIF-1. Genes Devel 13, 64–75. [PubMed: 9887100]

Borgia A, Borgia MB, Bugge K, Kissling VM, Heidarsson PO, Fernandes CB, Sottini A, Soranno A, Buholzer KJ, Nettels D, et al. (2018). Extreme disorder in an ultrahigh-affinity protein complex. Nature 555, 61–66. [PubMed: 29466338]

Brinkmann U, Mattes RE, and Buckel P (1989). High-level expression of recombinant genes in *Escherichia coli* is dependent on the availability of the dnaY gene product. Gene 85, 109–114. [PubMed: 2515992]

Chen T-Y, Cheng Y-S, Huang P-S, and Chen P (2018). Facilitated unbinding via multivalency-enabled ternary complexes: new paradigm for protein–DNA interactions. Acc. Chem. Res 51, 860–868. [PubMed: 29368512]

Chen T-Y, Santiago AG, Jung W, Krzemiński Ł, Yang F, Martell DJ, Helmann JD, and Chen P (2015). Concentration- and chromosome-organization-dependent regulator unbinding from DNA for transcription regulation in living cells. Nat. Commun 6, 7445. [PubMed: 26145755]

Chu W-T, Chu X, and Wang J (2020). Investigations of the underlying mechanisms of HIF-1α and CITED2 binding to TAZ1. Proc. Natl. Acad. Sci. U.S.A 117, 5595–5603. [PubMed: 32123067]

Dames SA, Martinez-Yamout M, De Guzman RN, Dyson HJ, and Wright PE (2002). Structural basis for Hif-1a/CBP recognition in the cellular hypoxic response. Proc. Natl. Acad. Sci. U.S.A 99, 5271–5276. [PubMed: 11959977]

De Guzman RN, Martinez-Yamout M, Dyson HJ, and Wright PE (2004). Interaction of the TAZ1 domain of CREB-binding protein with the activation domain of CITED2: regulation by competition between intrinsically unstructured ligands for non-identical binding sites. J. Biol. Chem 279, 3042–3049. [PubMed: 14594809]

De Guzman RN, Wojciak JM, Martinez-Yamout MA, Dyson HJ, and Wright PE (2005). CBP/p300 TAZ1 domain forms a structured scaffold for ligand binding. Biochemistry 44, 490–497. [PubMed: 15641773]

Delaglio F, Grzesiek S, Vuister GW, Guang Z, Pfeifer J, and Bax A (1995). NMRPipe: a multidimensional spectral processing system based on UNIX pipes. J. Biomol. NMR 6, 277–293. [PubMed: 8520220]

Drori I (2007). Fast l_1 minimization by iterative thresholding for multidimensional NMR spectroscopy. EURASIP Journal on Advances in Signal Processing 2007, 020248.

Eaton JW, Bateman D, Hauberg S, and Wehbring R (2021). GNU Octave version 6.2.0 manual: a high-level interactive language for numerical computations.

Ebert BL, and Bunn HF (1998). Regulation of transcription by hypoxia requires a multiprotein complex that includes hypoxia-inducible factor 1, an adjacent transcription factor, and p300/CREB binding protein. Mol. Cell. Biol 18, 4089–4096. [PubMed: 9632793]

Emsley P, Lohkamp B, Scott WG, and Cowtan K (2010). Features and development of Coot. Acta Cryst. D 66, 486–501. [PubMed: 20383002]

Freedman SJ, Sun ZY, Kung AL, France DS, Wagner G, and Eck MJ (2003). Structural basis for negative regulation of hypoxia-inducible factor-1a by CITED2. Nat. Struct. Biol 10, 504–512. [PubMed: 12778114]

Freedman SJ, Sun ZY, Poy F, Kung AL, Livingston DM, Wagner G, and Eck MJ (2002). Structural basis for recruitment of CBP/p300 by hypoxia-inducible factor-1a. Proc. Natl. Acad. Sci. U.S.A 99, 5367–5372. [PubMed: 11959990]

Graham JS, Johnson RC, and Marko JF (2010). Concentration-dependent exchange accelerates turnover of proteins bound to double-stranded DNA. Nucl. Acids Res 39, 2249–2259. [PubMed: 21097894]

Henze A-T, and Acker T (2010). Feedback regulators of hypoxia-inducible factors and their role in cancer biology. Cell Cycle 9, 2821–2835.

Huang LE, Gu J, Schau M, and Bunn HF (1998). Regulation of hypoxia-inducible factor 1a is mediated by an O_2-dependent degradation domain via the ubiquitin-proteasome pathway. Proc. Natl. Acad. Sci. U.S.A 95, 7987–7992. [PubMed: 9653127]

Iakoucheva LM, Brown CJ, Lawson JD, Obradovic Z, and Dunker AK (2002). Intrinsic disorder in cell-signaling and cancer-associated proteins. J. Mol. Biol 323, 573–584. [PubMed: 12381310]

Ivan M, Kondo K, Yang HF, Kim W, Valiando J, Ohh M, Salic A, Asara JM, Lane WS, and Kaelin WG Jr. (2001). HIFa targeted for VHL-mediated destruction by proline hydroxylation: Implications for O_2 sensing. Science 292, 464–468. [PubMed: 11292862]

Jaakkola P, Mole DR, Tian YM, Wilson MI, Gielbert J, Gaskell SJ, Kriegsheim A, Hebestreit HF, Mukherji M, Schofield CJ, et al. (2001). Targeting of HIF-a to the von Hippel-Lindau ubiquitylation complex by O_2-regulated prolyl hydroxylation. Science 292, 468–472. [PubMed: 11292861]

Joshi CP, Panda D, Martell DJ, Andoy NM, Chen T-Y, Gaballa A, Helmann JD, and Chen P (2012). Direct substitution and assisted dissociation pathways for turning off transcription by a MerR-family metalloregulator. Proc. Natl. Acad. Sci. U.S.A 109, 15121–15126. [PubMed: 22949686]

Kamar RI, Banigan EJ, Erbas A, Giuntoli RD, Olvera de la Cruz, M., Johnson, R.C., and Marko, J.F. (2017). Facilitated dissociation of transcription factors from single DNA binding sites. Proc. Natl. Acad. Sci. U.S.A 114, E3251–E3257. [PubMed: 28364020]

Kim B, Eggel A, Tarchevskaya SS, Vogel M, Prinz H, and Jardetzky TS (2012). Accelerated disassembly of IgE–receptor complexes by a disruptive macromolecular inhibitor. Nature 491, 613–617. [PubMed: 23103871]

Lee W, Tonelli M, and Markley JL (2015). NMRFAM-SPARKY: enhanced software for biomolecular NMR spectroscopy. Bioinformatics 31, 1325–1327. [PubMed: 25505092]

Lescop E, Schanda P, and Brutscher B (2007). A set of BEST triple-resonance experiments for time-optimized protein resonance assignment. J. Magn. Reson 187, 163–169. [PubMed: 17468025]

Liebschner D, Afonine PV, Baker ML, Bunkoczi G, Chen VB, Croll TI, Hintze B, Hung L-W, Jain S, McCoy AJ, et al. (2019). Macromolecular structure determination using X-rays, neutrons and electrons: recent developments in Phenix. Acta Cryst. D 75, 861–877.

Lindström I, Andersson E, and Dogan J (2018). The transition state structure for binding between TAZ1 of CBP and the disordered Hif-1α CAD. Sci. Rep 8, 7872. [PubMed: 29777197]

Liu J, Perumal NB, Oldfield CJ, Su EW, Uversky VN, and Dunker AK (2006). Intrinsic disorder in transcription factors. Biochemistry 45, 6873–6888. [PubMed: 16734424]

Love JJ, Li X, Chung J, Dyson HJ, and Wright PE (2004). The LEF-1 HMG domain undergoes a disorder-to-order transition upon complex formation with cognate DNA. Biochemistry 43, 8725–8734. [PubMed: 15236581]

Maciejewski MW, Schuyler AD, Gryk MR, Moraru II, Romero PR, Ulrich EL, Eghbalnia HR, Livny M, Delaglio F, and Hoch JC (2017). NMRbox: A Resource for Biomolecular NMR Computation. Biophys. J 112, 1529–1534. [PubMed: 28445744]

Nurwidya F, Takahashi F, Minakata K, Murakami A, and Takahashi K (2012). From tumor hypoxia to cancer progression: the implications of hypoxia-inducible factor-1 expression in cancers. Anat. Cell Biol 45, 73–78. [PubMed: 22822460]

Otwinowski Z, and Minor W (1997). Processing of x-ray diffraction data collected in oscillation mode. In Methods Enzymol Macromol. Crystall. A, Carter CW Jr., and Sweet RM, eds. (New York: Academic Press), pp. 307–326.

Potoyan DA, Bueno C, Zheng W, Komives EA, and Wolynes PG (2017). Resolving the NFkappaB Heterodimer Binding Paradox: Strain and Frustration Guide the Binding of Dimeric Transcription Factors. J. Am. Chem. Soc 139, 18558–18566. [PubMed: 29183131]

Rodriguez DD, Grosse C, Himmel S, Gonzalez C, de Ilarduya IM, Becker S, Sheldrick GM, and Uson I (2009). Crystallographic ab initio protein structure solution below atomic resolution. Nat. Methods 6, 651–653. [PubMed: 19684596]

Ruiz-Ortiz I, and De Sancho D (2020). Competitive binding of HIF-1α and CITED2 to the TAZ1 domain of CBP from molecular simulations. Phys. Chem. Chem. Phys 22, 8118–8127. [PubMed: 32242581]

Sammito M, Millán C, Frieske D, Rodríguez-Freire E, Borges RJ, and Usón I (2015). ARCIMBOLDO_LITE: single-workstation implementation and use. Acta Crystallographica D 71, 1921–1930.

Sattler M, Schleucher J, and Griesinger C (1999). Heteronuclear multidimensional NMR experiments for the structure determination of proteins in solution employing pulsed field gradients. Prog. NMR Spect 34, 93–158.

Schanda P, VanMelckebeke H, and Brutscher B (2006). Speeding Up Three-Dimensional Protein NMR Experiments to a Few Minutes. J. Am. Chem. Soc 128, 9042–9043. [PubMed: 16834371]

Schmitt L, Kratz JR, Davis MM, and McConnell HM (1999). Catalysis of peptide dissociation from class II MHC-peptide complexes. Proc. Natl. Acad. Sci. U.S.A 96, 6581–6586. [PubMed: 10359754]

Semenza GL (2014). Oxygen sensing, hypoxia-inducible factors, and disease pathophysiology. Annu. Rev. Pathol. Mech. Dis 9, 47–71.

Sottini A, Borgia A, Borgia MB, Bugge K, Nettels D, Chowdhury A, Heidarsson PO, Zosel F, Best RB, Kragelund BB, et al. (2020). Polyelectrolyte interactions enable rapid association and dissociation in high-affinity disordered protein complexes. Nat. Commun 11, 5736. [PubMed: 33184256]

Stern AS, Donoho DL, and Hoch JC (2007). NMR data processing using iterative thresholding and minimum l1-norm reconstruction. J. Magn. Reson 188, 295–300. [PubMed: 17723313]

Sugase K, Landes MA, Wright PE, and Martinez-Yamout M (2008). Overexpression of post-translationally modified peptides in *Escherichia coli* by co-expression with modifying enzymes. Prot. Express. Purif 57, 108–115.

Tsai M-Y, Zhang B, Zheng W, and Wolynes PG (2016). Molecular Mechanism of Facilitated Dissociation of Fis Protein from DNA. J. Am. Chem. Soc 138, 13497–13500. [PubMed: 27685351]

Wang GL, Jiang B, Rue EA, and Semenza GL (1995). Hypoxia-inducible factor 1 is a basic-helix-loop-helix-PAS heterodimer regulated by cellular O_2 tension. Proc. Natl. Acad. Sci. U.S.A 92, 5510–5514. [PubMed: 7539918]

Wang Y, and Brooks CL (2020). Electrostatic forces control the negative allosteric regulation in a disordered protein switch. J. Phys. Chem. Lett 11, 864–868. [PubMed: 31940206]

Williams CJ, Headd JJ, Moriarty NW, Prisant MG, Videau LL, Deis LN, Verma V, Keedy DA, Hintze BJ, Chen VB, Jain S, Lewis SM, Arendall WB 3rd, Snoeyink J, Adams PD, Lovell SC, Richardson JS, Richardson DC (2018). MolProbity: More and better reference data for improved all-atom structure validation. Protein Sci 27, 293–315/ [PubMed: 29067766]

Wright PE, and Dyson HJ (2015). Intrinsically disordered proteins in cellular signalling and regulation. Nat. Rev. Mol. Cell Biol 16, 18–29. [PubMed: 25531225]

Highlights:

- Mechanistic insights into regulation of the hypoxic response
- Molecular determinants for displacement of HIF-1α by facilitated dissociation
- Fusion protein strategy to characterize a model of a transient ternary complex
- Structural analysis of a negative allosteric network involving disordered proteins

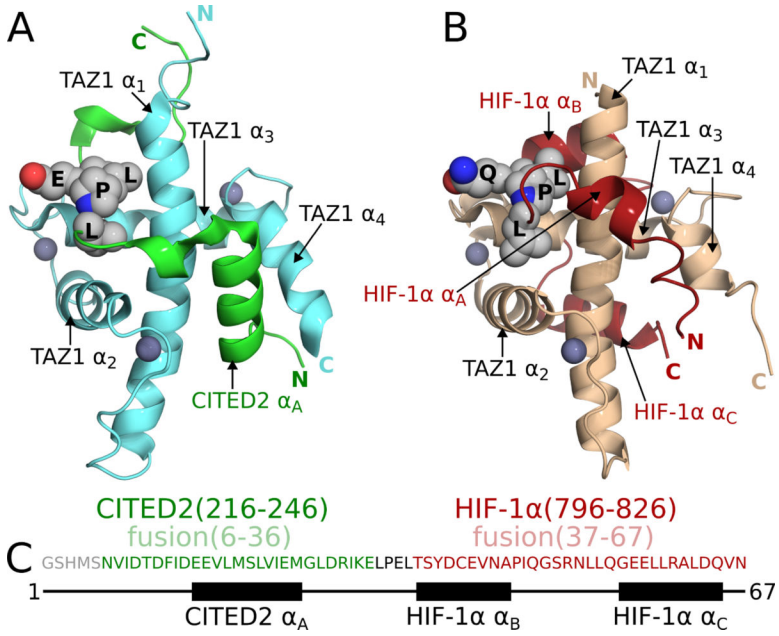

Figure 1. TAZ1:CITED2 and TAZ1:HIF-1α structures and the design of a CITED2-HIF-1α fusion.

(A) NMR structure of the TAZ1:CITED2 complex (PDB 1R8U; (De Guzman et al., 2004)). TAZ1(CBP 340–439) is shown in cyan and CITED2(220–269) is shown in green. Zinc atoms are shown as dark-gray spheres. Side chains of the CITED2 LPEL motif are shown as light-gray spheres with N and O atoms colored blue and red respectively. Black labels are superimposed on the LPEL side chains. TAZ1 and CITED2 helices and N- and C-termini are labeled for reference. Residues 262–269 of CITED2 are omitted for clarity. (B) NMR structure of the TAZ1:HIF-1α complex (PDB 1L8C; (Dames et al., 2002)). TAZ1(CBP 345–439) is shown in tan and HIF1α(776–826) is shown in red. Zinc atoms are shown as dark-gray spheres. Side chains of the HIF-1α LPQL motif are shown as light-gray spheres with N and O atoms colored blue and red respectively. Black labels are superimposed on the LPQL side chains. TAZ1 and HIF-1α helices and N- and C-termini are labeled for reference. (C) Amino acid sequence of the fusion peptide. Sequences from CITED2 (residues 216–246) and HIF-1α (residues 796–826) are colored green and red respectively and correspond to residues 6–36 and 37–67 of the fusion peptide. The LPEL motif of the CITED2 sequence is shown in black. The N-terminal GSHMS sequence is a cloning artifact (see methods). The block diagram below the sequence denotes the positions of the CITED2 and HIF-1α helical binding motifs.

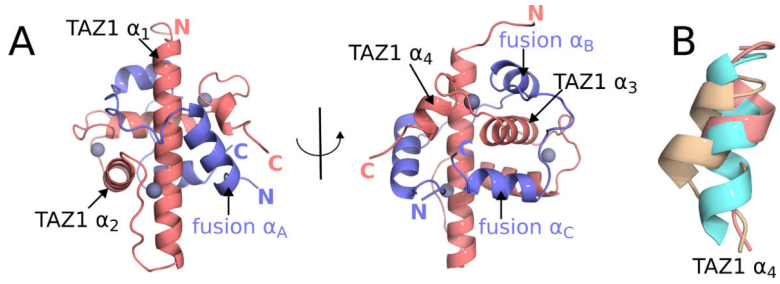

Figure 2. Crystal structure of the TAZ1:fusion peptide complex and conformation of the TAZ1 α_4 helix.

(A) Crystal structure of the TAZ1:fusion peptide complex. TAZ1 is shown in salmon and the fusion peptide is shown in slate. Zinc atoms are shown as gray spheres. TAZ1 and fusion peptide helices and N- and C-termini are labeled for reference. (B) Superpositions of the TAZ1 α_4 helix from the TAZ1:CITED2 (cyan), TAZ1:HIF-1α (tan), and TAZ1:fusion peptide (salmon) structures. Structures were aligned based on residues from the TAZ1 α_1 (residues 350–363), α_2 (residues 383–397), and α_3 (residues 407–420) helices. Residues 426–437, encompassing the TAZ1 α_4 helix, are shown.

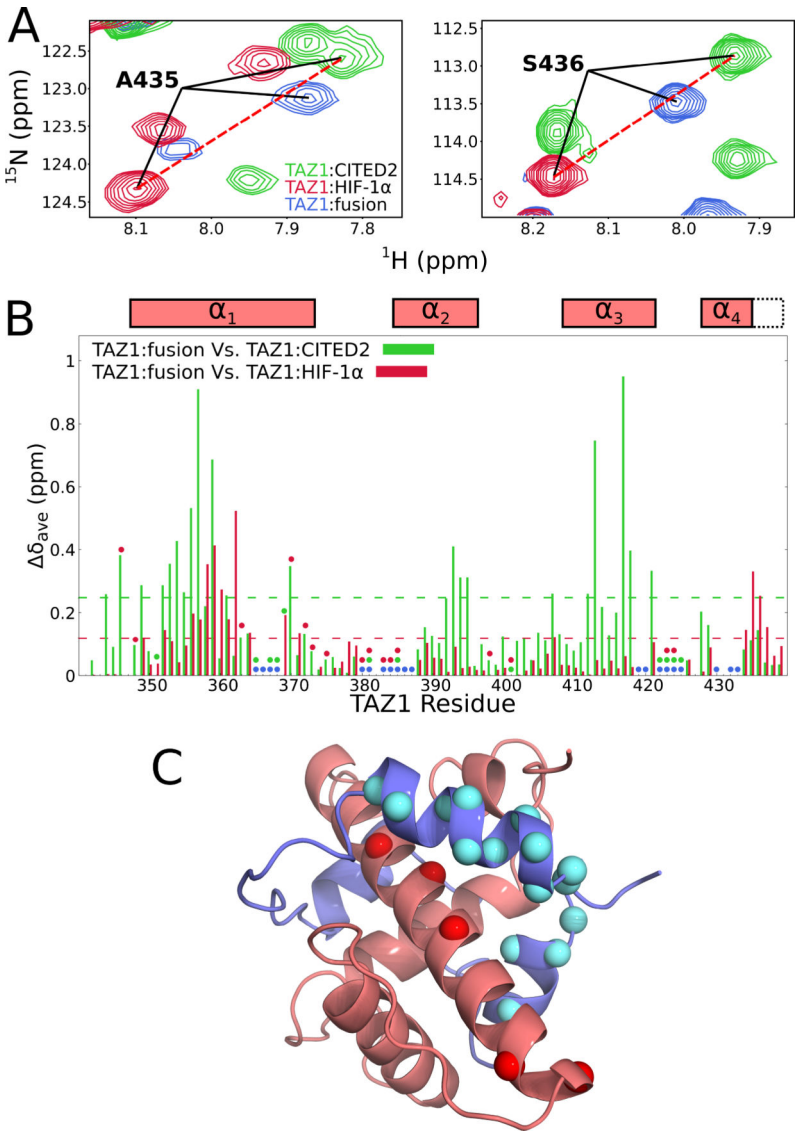

Figure 3. Comparison of ^{1}H-^{15}N HSQC spectra of ^{15}N-labeled TAZ1 in complex with CITED2, HIF-1α, and the fusion peptide.

(A) Regions of superimposed ^{1}H-^{15}N HSQC spectra (900 MHz ^{1}H frequency) of ^{15}N-labeled TAZ1 bound to unlabeled CITED2 (green), HIF-1α (red), or fusion peptide (blue). Backbone amide cross peaks corresponding to TAZ1 α_4 helix residues A435 (left panel) and S436 (right panel) are labeled. (B) Weighted average ^{1}H,^{15}N chemical shift differences for ^{15}N-TAZ1 ($\Delta\delta_{ave}=[(\Delta\delta_{HN})^2+(\Delta\delta_N/5)^2]^{½}$) between the CITED2 and fusion peptide complexes (green) and between the HIF-1α and fusion peptide complexes (red). Circles denote residues for which backbone amide resonance assignments are missing for the CITED2 (green), HIF-1α (red), and fusion peptide (blue) complexes. Residues for which there are no circles and no data are prolines. Boxes above the plot indicate the positions of the TAZ1 α_1 − α_4 helices in the TAZ1:fusion peptide crystal structure; the broken lines indicate the length of the α_4 helix in the TAZ1:CITED2 structure. The broken green and red lines inside the graph denote one standard deviation above the 10 % trimmed mean for the

TAZ1:CITED2 Vs. TAZ1:fusion peptide and TAZ1:HIF-1α Vs. TAZ1:fusion peptide data sets, respectively. (C) Structure of the TAZ1:fusion peptide complex, with TAZ1 shown in salmon and the fusion peptide in slate. TAZ1 α_1 residues for which backbone amide ^{1}H-^{15}N HSQC cross peak intensity is reduced by greater than 60 % in the fusion peptide complex compared to the CITED2 complex are shown as red spheres. Fusion peptide α_A and α_C residues for which backbone amide resonances are broadened beyond detection or have normalized cross peak intensity less than 0.2 (see Figure 4B) are shown as cyan spheres. Zn atoms are omitted for clarity.

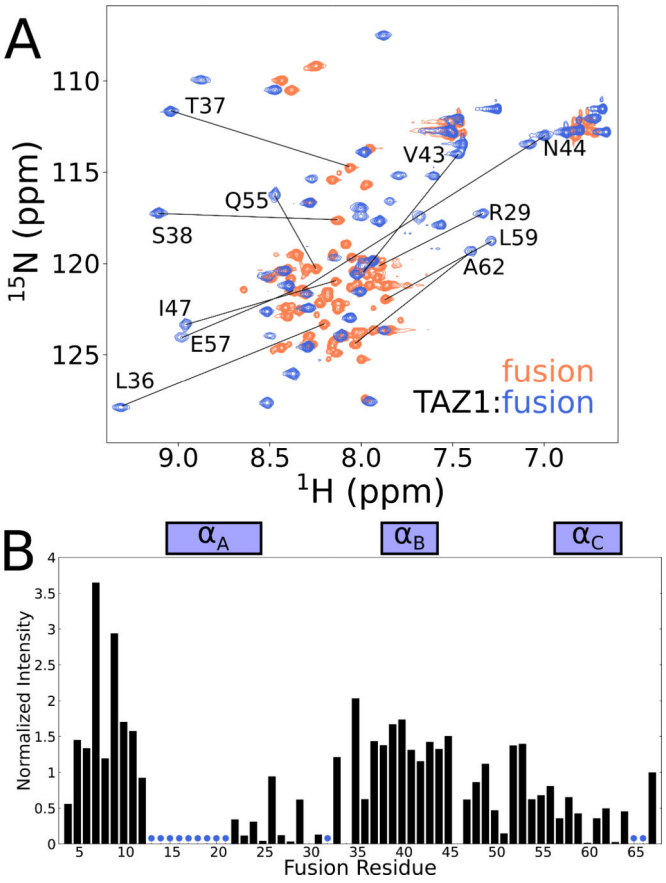

Figure 4. Solution NMR characterization of the fusion peptide.

(A) Superimposed 900 MHz ^{1}H-^{15}N HSQC spectra of ^{15}N-labeled fusion peptide bound to unlabeled TAZ1 (blue) and free in solution (coral). Representative amide cross peaks that undergo large shifts in position upon complex formation are labeled. (B) Intensities of backbone amide cross peaks from ^{1}H-^{15}N HSQC spectra of ^{15}N-labeled fusion peptide in complex with unlabeled TAZ1. Intensities are normalized to the intensity of the backbone amide cross peak of the C-terminal fusion peptide residue (N67). Boxes above the plot indicate the positions of the CITED2 α_A and HIF1α α_B and α_C binding motifs. Residues for which backbone amide cross peaks are broadened beyond detection are denoted by blue circles.

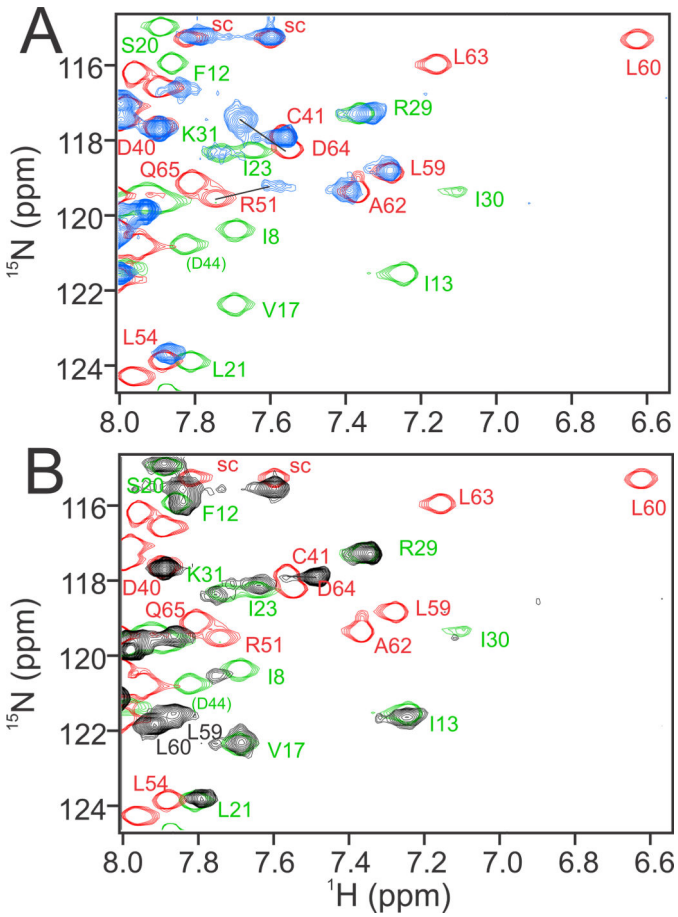

Figure 5. Comparison of ^{1}H-^{15}N HSQC spectra of ^{15}N-labeled CITED2, HIF-1α, and fusion peptides in complex with TAZ1.

(A) Overlay of a region of the spectra of ^{15}N-labeled fusion peptide (blue), ^{15}N-labeled CITED2 (green), and ^{15}N-labeled HIF-1α (red) bound to unlabeled TAZ1. (B) Overlay of a region of the spectra of ^{15}N-labeled L63A fusion peptide(black) ^{15}N-labeled CITED2 (green), and ^{15}N-labeled HIF-1α (red) bound to unlabeled TAZ1. Cross peaks from the CITED2 and HIF-1α complexes are shown with only the outer contours for clarity and, in panel A, are connected by lines to the corresponding cross peaks of the fusion peptide complex. Cross peaks from the N-terminus of the HIF-1α complex and the C-terminus of the CITED2 complex have no corresponding cross peak in the fusion peptide complex spectrum and are labeled in smaller font in parentheses. The cross peaks of an amide side chain are denoted sc.

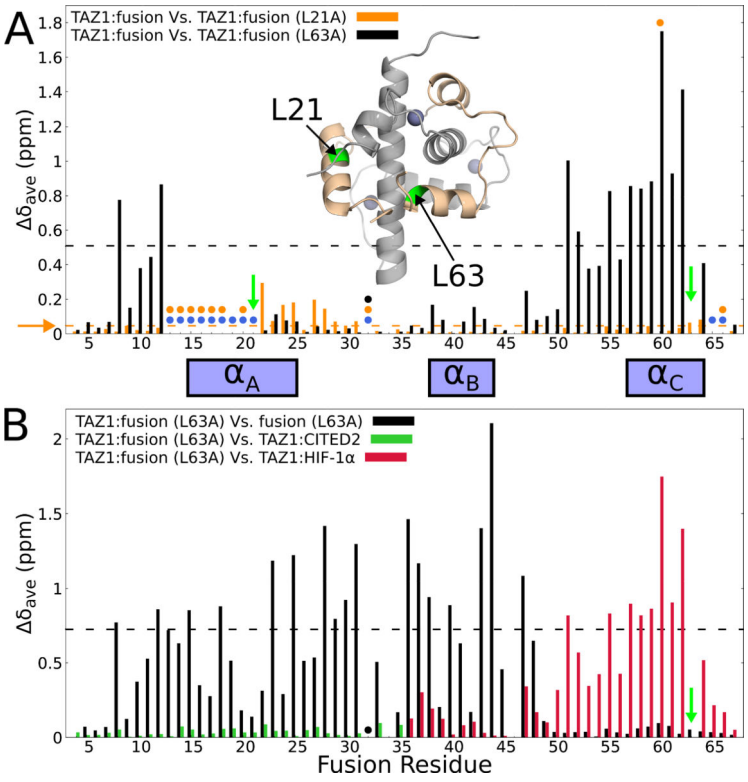

Figure 6. Site-directed mutagenesis to probe TAZ1-mediated allosteric interactions between the fusion peptide α_A and α_C helices.

(A) Weighted average $^{1}H,^{15}N$ chemical shift differences between the original ^{15}N-labeled fusion peptide in complex with unlabeled TAZ1 and ^{15}N-labeled L21A (orange) or ^{15}N-labeled L63A (black) fusion peptide in complex with unlabeled TAZ1. Green arrows indicate the sites of mutation. Circles denote residues for which backbone amide cross peaks are broadened beyond detection for the TAZ1 complexes of the original fusion peptide (blue), L21A fusion peptide (orange), and L63A fusion peptide (black). Residues for which there are no circles and no data are prolines. The broken horizontal lines (and horizontal orange arrow) denote one standard deviation above the 10 % trimmed mean for the TAZ1:fusion vs. TAZ1:fusion (L21A) (orange) and TAZ1:fusion vs. TAZ1:fusion (L63A) (black) data sets. Inset: structure of the fusion peptide complex, with TAZ1 shown in gray and the fusion peptide shown in tan. Residues L21 and L63 are labeled and colored green. Zn atoms are shown as gray spheres. (B) Weighted average $^{1}H,^{15}N$ chemical shift differences for the TAZ1-bound L63A fusion peptide relative to the unbound state (black), to residues 220–245 of CITED in complex with TAZ1 (green, corresponding to residues 10–35 of the fusion peptide), and to residues 795–826 of HIF-1α in complex with TAZ1 (red, corresponding to residues 36–67 of the fusion peptide).The green arrow indicates the site of mutation. The backbone amide resonance corresponding to E32 is broadened beyond detection and is marked with a black circle. The broken black line denotes one standard deviation above the 10 % trimmed mean of the TAZ1:fusion (L63A) vs. free L63A fusion peptide shift differences. The boxes between panels A and B denote the positions of the CITED2 α_A and HIF-1α α_B and α_C binding motifs.

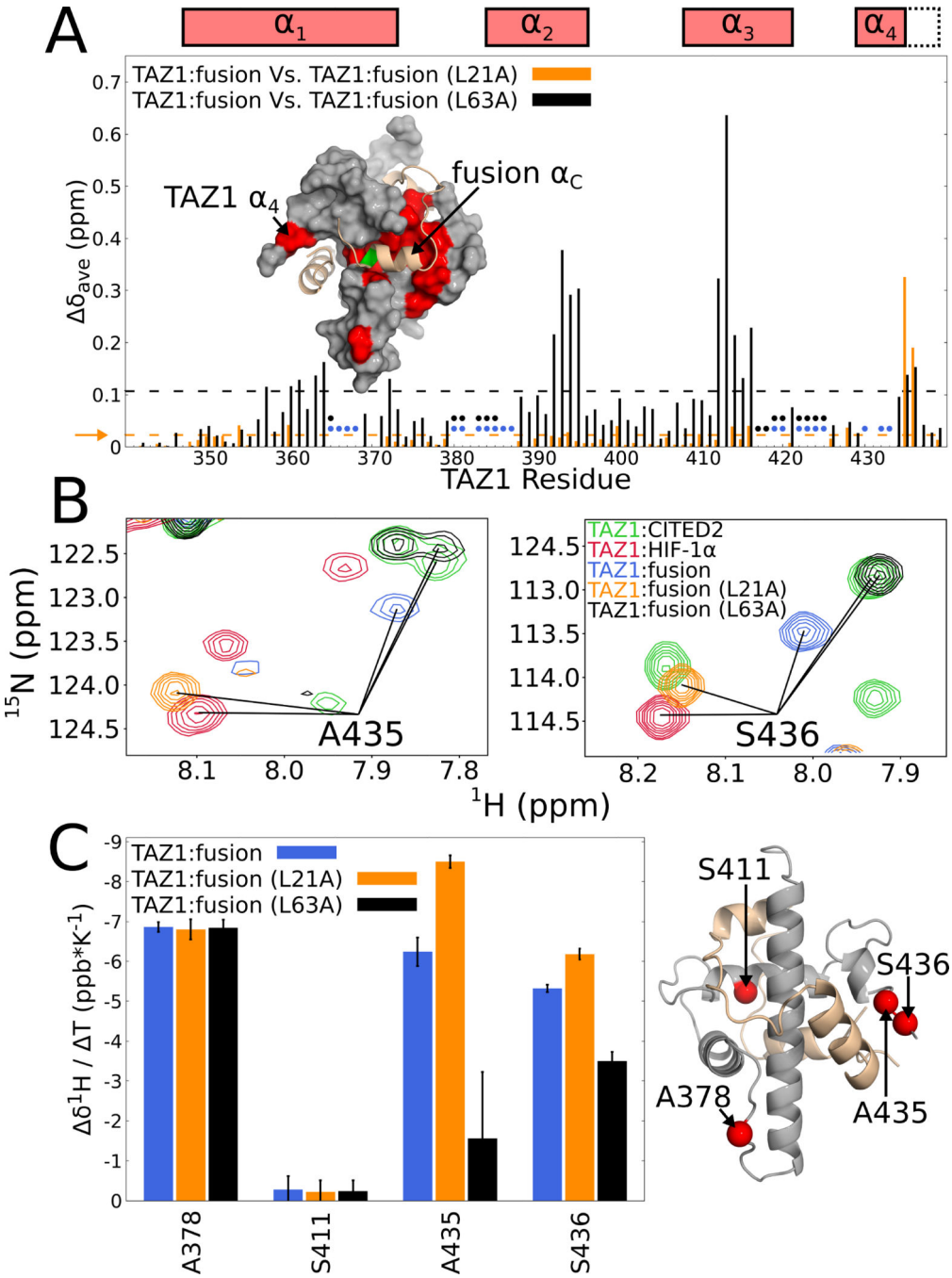

Figure 7. Effects of fusion peptide L21A and L63A mutations on TAZ1 resonances.

(A) Weighted average ^{1}H,^{15}N chemical shift differences for TAZ1 amide cross peaks in complex with unlabeled fusion peptide relative to the L21A (orange) or L63A (black) fusion peptide complexes. The broken orange and black lines and the horizontal orange arrow denote one standard deviation above the 10 % trimmed mean of the L21A and L63A fusion peptide histograms, respectively. The circles indicate residues for which TAZ1 backbone amide cross peaks are weak or missing in spectra of the original fusion peptide (blue) and the L63A fusion peptide (black) complexes. Backbone amide cross peaks of ^{15}N-labeled

TAZ1 in complex with unlabeled L21A fusion peptide were assigned based on the similarity of chemical shifts in spectra of the original fusion peptide complex. Missing assignments are mostly associated with cross peaks in highly overlapped regions of the spectrum. Inset: TAZ1:fusion peptide structure, with TAZ1 shown as a gray surface and the bound fusion peptide as a tan cartoon with L63 highlighted in green. Residues for which the weighted average TAZ1 chemical shift differences between the original fusion peptide and L63A fusion peptide complexes (panel A) are greater than one standard deviation above the 10 % trimmed mean are colored red. Boxes above the plot denote positions of the TAZ1 α_1 – α_4 helices in the TAZ1:fusion peptide crystal structure, with dotted lines indicating the extended α_4 helix in the TAZ1:CITED2 structure. (B) Overlays of ^{1}H-^{15}N HSQC spectra (900 MHz ^{1}H frequency) of ^{15}N-labeled TAZ1 in complex with unlabeled CITED2 (green), HIF-1α (red), fusion peptide (blue), L21A fusion peptide (orange), or L63A fusion peptide (black). Cross peaks corresponding to the backbone amides of A435 and S436 are labeled in the left and right panels respectively. (C) Left: Temperature coefficients of backbone amide proton resonances of residues A378, S411, A435, and S436 of TAZ1 in complex with the original (blue), L21A (orange), or L63A (black) fusion peptide. Error bars represent the 68 % confidence interval of the fitted slope. Right: Structure of the TAZ1:fusion peptide complex showing the locations of A378, S411, A435, and S436 as red spheres. Zn atoms are omitted for clarity.

KEY RESOURCES TABLE

REAGENT or RESOURCE	SOURCE	IDENTIFIER
Antibodies		
Bacterial and Virus Strains		
E. coli BL21 (DE3)	Agilent	F– *ompT hsdSB* (*rB* – *mB* –) *gal dcm* (DE3)
E. coli XL-1 Blue competent cells	Agilent	*recA1 endA1 gyrA96 thi-1 hsdR17 supE44 relA1 lac* [F´ *proAB lacI*^{q}*ZΔM15* Tn*10* (Tet^{r})]
Biological Samples		
Chemicals, Peptides, and Recombinant Proteins		
TAZ1 domain of *M. musculus* CREB-binding protein	This paper	N/A
H. sapiens Hypoxia inducible factor 1α C-terminal activation domain	This paper	N/A
H. sapiens CITED2 C-terminal activation domain	This paper	N/A
H. sapiens CITED2 C-terminal activation domain - *H. sapiens* Hypoxia inducible factor 1α C-terminal activation domain fusion peptide	This paper	N/A
H. sapiens CITED2 C-terminal activation domain - *H. sapiens* Hypoxia inducible factor 1α C-terminal activation domain fusion peptide L21A-mutant	This paper	N/A
H. sapiens CITED2 C-terminal activation domain - *H. sapiens* Hypoxia inducible factor 1α C-terminal activation domain fusion peptide L63A-mutant	This paper	N/A
Critical Commercial Assays		
Deposited Data		
Crystal structure of the CREB-binding protein TAZ1 domain in complex with a CITED2 C-terminal activation domain - Hypoxia inducible factor 1α C-terminal activation domain fusion peptide	This paper	PDB 7LVS
NMR solution structure of the CREB-binding protein TAZ1 domain in complex with a CITED2 C-terminal activation domain	De Guzman et al., 2004	PDB 1R8U
NMR solution structure of the CREB-binding protein TAZ1 domain in complex with a Hypoxia inducible factor 1α C-terminal activation domain	Dames et al., 2002	PDB 1L8C
NMR solution structure of TAZ1	De Guzman et al., 2005	PDB 1U2N
Backbone chemical shift assignments: CITED2 C-terminal activation domain - Hypoxia inducible factor 1α C-terminal activation domain fusion peptide	This paper	BMRB 50866
Backbone chemical shift assignments: CITED2 C-terminal activation domain - Hypoxia inducible factor 1α C-terminal activation domain fusion peptide in complex with the CREB-binding protein TAZ1 domain: TAZ1	This paper	BMRB 50865
Backbone chemical shift assignments: CITED2 C-terminal activation domain - Hypoxia inducible factor 1α C-terminal activation domain fusion peptide in complex with the CREB-binding protein TAZ1 domain: fusion peptide	This paper	BMRB 50865
Backbone chemical shift assignments: CITED2 C-terminal activation domain - Hypoxia inducible factor 1α C-terminal activation domain fusion peptide L63A mutant in complex with the CREB-binding protein TAZ1 domain: TAZ1	This paper	BMRB 50867
Backbone chemical shift assignments: CITED2 C-terminal activation domain - Hypoxia inducible factor 1α C-terminal activation domain fusion peptide L63A mutant in complex with the CREB-binding protein TAZ1 domain: fusion peptide	This paper	BMRB 50867
Experimental Models: Cell Lines		
Experimental Models: Organisms/Strains		
Oligonucleotides		

REAGENT or RESOURCE	SOURCE	IDENTIFIER
PCR Primer: 5'-gtccgcggtgatagaaatgggtttggaccgcatcaaggag (fusion peptide L21A mutation)	This paper; Integrated DNA Technologies	N/A
PCR Primer: 5'-caaacccatttctatcaccgcggacataagaacttcctcgtcgatgaaatcagtg (fusion peptide L21A mutation)	This paper; Integrated DNA Technologies	N/A
PCR Primer: 5'-gctgcggatcaagttaactgatagggatcccctctagaaa (fusion peptide L63A mutation	This paper; Integrated DNA Technologies	N/A
PCR Primer: 5'-aacttgatccgcagctctgagtaattcttcaccctgcag (fusion peptide L63A mutation)	This paper; Integrated DNA Technologies	N/A
Recombinant DNA		
pET21d encoding *M. musculus* CREB-binding protein TAZ1 domain	De Guzman et al., 2005	Addgene #173760
dnaY	Love et al., 2004, Brinkmann et al., 1989	N/A
pET22b encoding *M. musculus* CREB-binding protein TAZ1 domain and the His_6-tagged B1 domain of streptococcal protein G fused to the C-terminal activation domain of *H. sapiens* hypoxia-inducible factor 1α	Sugase et al., 2008	Addgene #99343
pET22b encoding *M. musculus* CREB-binding protein TAZ1 domain and the His_6-tagged B1 domain of streptococcal protein G fused to the C-terminal activation domain of *H. sapiens* CITED2	Berlow et al., 2017	Addgene #173761
pET22b encoding *M. musculus* CREB-binding protein TAZ1 domain and the His_6-tagged B1 domain of streptococcal protein G fused to a *H. sapiens* CITED2 C-terminal activation domain – *H. sapiens* hypoxia-inducible factor 1α C-terminal activation domain fusion	This manuscript	Addgene #173762
pET22b encoding *M. musculus* CREB-binding protein TAZ1 domain and the His_6-tagged B1 domain of streptococcal protein G fused to a *H. sapiens* CITED2 C-terminal activation domain – *H. sapiens* hypoxia-inducible factor 1α C-terminal activation domain fusion harboring the L21A mutation	This manuscript	Addgene #173763
pET22b encoding *M. musculus* CREB-binding protein TAZ1 domain and the His_6-tagged B1 domain of streptococcal protein G fused to a *H. sapiens* CITED2 C-terminal activation domain – *H. sapiens* hypoxia-inducible factor 1α C-terminal activation domain fusion harboring the L63A mutation	This manuscript	Addgene #173764
Software and Algorithms		
NmrPipe	Delaglio et al., 1995	https://www.ibbr.umd.edu/nmrpipe/install.html
NMRbox	Maciejewski et al., 2017	https://nmrbox.org
NMRFAM-SPARKY	Lee et al., 2015	https://nmrfam.wisc.edu/nmrfam-sparky-distribution
Bruker Topspin 3.2	www.Bruker.com	https://www.bruker.com/en/products-and-solutions/mr/nmr-software/topspin.html
Bruker XWIN-NMR 3.1	www.Bruker.com	www.Bruker.com
Phenix	Liebschner et al., 2019	https://www.phenix-online.org
Coot	Emsley et al., 2010	https://www2.mrc-lmb.cam.ac.uk/personal/pemsley/coot
HKL-2000	Otwinowski and Minor, 1997	https://www.hkl-xray.com
Arcimboldo Lite	Sammito et al., 2015	chango.ibmb.csic.es/lite
Pymol	https://pymol.org/2/	https://pymol.org/2/

REAGENT or RESOURCE	SOURCE	IDENTIFIER
gnuplot	www.gnuplot.info	www.gnuplot.info
GNU Octave	Eaton et al., 2021	https://octave.org/doc/v6.2.0/
Other		

Table 1.

X-ray diffraction data collection and refinement statistics for the TAZ1:fusion peptide complex

Data collection [a]	
Beamline	ALS 5.0.3
Wavelength (Å)	0.97648
Resolution range (Å)	40.7–2.0
Space Group	$P2_1$
Unit cell dimensions (Å, °)	32.06,50.11,41.26; β=99.19
Total reflections	60265(3547)
Unique reflections	8465(562)
R_{merge} (%)[b]	11.1(145.5)
R_{meas} (%)[c]	12.0(158.6)
R_{pim} (%)[d]	4.5(62.4)
$CC_{1/2}$ (%)[e]	87.8(91.0)
Completeness (%)	100.0(99.8)
Redundancy	7.1(6.4)
$\langle I \rangle / \langle \sigma(I) \rangle$	17.9(1.2)
Refinement	
Reflections used for R_{work}(R_{free})	7543(882)
Number of non-H protein atoms	1214
Number of water molecules	36
Number of Zn atoms	3
R_{work}	0.2107
R_{free}	0.2406
RMS (bond length)	0.003
RMS (bond angle)	0.645
Ramachandran: favored, outliers (%)	95.36,0.66
Clashscore	5.78
Wilson B-factor (Å^2)	38.4
Average B-factor (Å^2)	65

[a] Values in parentheses are for highest resolution shell

[b] $R_{merge} = \Sigma_{hkl}\Sigma_{i=1,n}|I_i(hkl) - \langle I(hkl)\rangle| / \Sigma_{hkl}\Sigma_{i=1,n}I_i(hkl)$

[c] $R_{mease} = \Sigma_{hkl}\sqrt{(n/(n-1))}\Sigma_{i=1,n}|I_i(hkl) - \langle (I(hkl)\rangle| / \Sigma_{hkl}|\Sigma_{i=1,n}I_i(hkl)$

[d] $R_{pim} = \Sigma_{hkl}\sqrt{(1/(n-1))}\Sigma_{i=1,n}|I_i(hkl) - \langle I(hkl)\rangle| / \Sigma_{(hkl)}\Sigma_{i=1,n}I_i=(hkl)$

[e] $CC_{1/2}$ = Pearson Correlation Coefficient between two random half datasets

[f] Number of unfavorable all-atom steric overlaps ≥ 0.4 Å per 1000 atoms